Experimental and Numerical Investigation of the Impacts of Rotor Tip-Rake on Excitation Forces of Pump-Jet Propulsors

Xue-Qin Ji

jixueqin@sjtu.edu.cn

Shanghai Jiao Tong University

Xiao-Song Zhang

China Ship Scientific Research Center

Chen-Jun Yang

Shanghai Jiao Tong University https://orcid.org/0000-0002-6284-0772

Xiao-Qian Dong

Shanghai Jiao Tong University

Research Article

Keywords: Pump-jet, tip-clearance, tip-rake, fluctuating pressures, excitation forces

Posted Date: September 12th, 2023

DOI: https://doi.org/10.21203/rs.3.rs-3315287/v1

Version of Record: A version of this preprint was published at Journal of Hydrodynamics on April 11th, 2024. See the published version at https://doi.org/10.1007/s42241-024-0011-0.

Experimental and Numerical Investigation of the Impacts of Rotor Tip-Rake on Excitation Forces of Pump-Jet Propulsors

Xue-Qin Ji[1], Xiao-Song Zhang[2,3], Chen-Jun Yang[1,*], Xiao-Qian Dong[1]

1. State Key Laboratory of Ocean Engineering, Marine Numerical Experiment Centre, School of Naval Architecture, Ocean and Civil Engineering, Shanghai Jiao Tong University, Shanghai 200240, China.

2. CSSC Shanghai Marine Energy Saving Technology Co.,Ltd. Shanghai 200011, China

3. China Ship Scientific Research Center Shanghai Branch, Shanghai 200011, China

[*]Corresponding author. E-mail address: cjyang@sjtu.edu.cn (C.-J. Yang).

Abstract

The tip-clearance flow in a pump-jet propulsor exerts great impacts on the fluctuating pressures and resultant unsteady forces, which are important sources of structural vibrations and radiated noise underwater. The blade geometry close to the tip is an important factor determining the vortex strength in the tip-clearance flow. In the open-water condition, the effects of raking the rotor tips on duct-surface fluctuating pressures and the resultant unsteady forces acting on different components of the propulsor are investigated via physical model experiments and the numerical solution of Reynolds-Averaged Navier-Stokes equations coupled with the SST k-ω turbulence model. The measured and simulated results of hydrodynamic pressures are consistent to each other, and the simulated flows help better understand why the fluctuating pressures change with the tip geometry. The strong fluctuations of duct-surface pressures are caused by intensive tip separation vortices. The duct-surface pressure fluctuations are effectively reduced by using the rake distribution near the tip towards blade back side and, for the combination of the five-bladed rotor and the seven-bladed stator, the resultant unsteady horizontal (and vertical) forces acting on the duct and stator are also reduced. While increasing rake leads to negative effect on pressure fluctuations and unsteady horizontal (and vertical) forces acting on all the components of the propulsor.

Keywords: Pump-jet; tip-clearance; tip-rake; fluctuating pressures; excitation forces

1. Introduction

The pump-jet is a typical multi-component propulsor, where the interaction between the stationary and rotating parts of it induces periodically varying hydrodynamic loads that serve as a source of propulsor and/or hull-structure vibration and radiated noise. The non-uniform inflow and cavitation would further worsen the situation. Reducing the unsteady hydrodynamic loads, which originate from the fluctuating pressures acting on the duct and blade surfaces of the propulsor, is often an important objective of the design.

Many attempts have been made to reduce the fluctuating pressures and unsteady forces of the pump structures. For example, Yu et al. (2020) numerically investigated the impacts of stator chord length, pre-swirl angle and stator/rotor spacing on the unsteady forces arising from rotor/stator interactions. They showed that excessively increasing the pre-swirl angle could

increase the unsteady forces, while properly increasing the stator/rotor spacing could reduce the unsteady forces significantly. Sonawat et al. (2022) found that the use of staggered impeller design and split volute could effectively reduce the pressure fluctuations in the double suction centrifugal pump via experiments and CFD simulations.

In addition to studies on the primary parameters of rotor and stator blades, many researches focused on the impacts of tip-clearance flow on unsteady hydrodynamic loads. Different vortex structures exist near the rotor tips due to the tip-clearance flow, such as the tip-leakage vortex (TLV) and the tip-separation vortex (TSV), see Decaix et al. (2018). It was also found that the occurrence of hydrodynamic cavitation could lead to structural vibration (Karn et al., 2016) and flow instabilities (Arndt et al., 1991). In the experimental and numerical studies on a single volute vaneless centrifugal pump, González et al. (2005) found that reducing the radial gap by 5% could make the unsteady forces increase by 10%, and a wider gap gave rise to weaker unsteady forces. Chen et al. (2016) found the fluctuating pressure at the tip clearance was much larger than that at the inlet and outlet of the axial-flow pump using the numerical method of large eddy simulation. At the same time, the pump vibration and sound field were solved using the vibro-acoustic model and the frequency spectrum characteristics were consistent with those of pressure fluctuation. It could be inferred that the analysis of pressure fluctuation is an effective way to indirectly study the vibration and noise. Liu and Tan (2018) explored the influence of tip clearance on pressure fluctuation intensity and vortex characteristic of a mixed flow pump as turbine at pump mode. The turbulent flow characteristic was remarkably influenced by the tip clearance since the distribution of pressure fluctuation intensity on blade pressure side presented a triangular shape under design flow rate. When it comes to pump-jet propulsors, Yu et al. (2019) found that the pressure fluctuations increase significantly on rotor blade surfaces with the increase of tip clearance size, especially on the tip, root and leading edge of the blade. Meanwhile, the amplitudes of thrust and torque fluctuations increase as the tip clearance enlarges.

Except for the tip-clearance size, the blade geometry close to rotor blade tips is another factor determining the strength of vortex flow in the tip clearance. In Liu et al. (2018), typical tip geometries were reviewed, mostly for hydraulic machines such as pumps and turbines. Li et al. (2014) varied the width and thickness of the tip vanes and found that the fluctuating pressures on the shroud of a pump decreased initially but increased afterwards as the width was increased. Zhang et al. (2019) attempted to reduce the unsteady pressure pulsations in a centrifugal pump by modifying the blade trailing edge profile and concluded that pressure amplitudes of the modified profile were reduced obviously for major flow rates. Guo et al. (2016), Tan et al. (2018), Liu and Tan (2020) investigated different tip shapes of the impeller. It was found that the sharp tip foil reduced the tip-leakage flow losses and strengthened the separation vortex compared to round tip foil. On the other hand, Liu and Tan. (2018), Cheng et al. (2020), Ye et al. (2021) investigated different groove structures applied to the tip, such as the C-type, the overhanging type, and the rectangular type, to suppress the TLV in pumps and pump-jet propulsors. Ji et al. (2019, 2021) investigated a simple way of weakening the TLV of the pump-jet propulsor which is raking the rotor tips towards blade face side in the region beyond 95% tip radius. It was found through CFD simulations that both the TLV strength and pressure fluctuations in TLV core were reduced by a large amount. However, the TSVs became stronger, which was unfavorable for cavitation inception at least, and might induce other adverse effects.

Special geometry of the tip is worth investigation not only for weakening the tip-clearance flow but also for reducing the unsteady hydrodynamic loads.

In general, few researches are carried out on the fluctuation characteristics of pump-jet propulsors rather than pumps, and most of the existing researches are based on numerical simulation methods, lacking reliable test verification analysis. In current research, the impacts of backward rake and forward rake on duct-surface fluctuating pressures and resultant unsteady forces (due to stator/rotor interaction in the open-water and without cavitation) are investigated via physical model experiments and CFD simulations. In the following, the design of tip-geometry, the experimental study and the numerical study are expounded in Sections 2, 3 and 4, respectively. The main conclusions are given in Section 5.

2. Design of Rotor-Tip Geometry

Three pump-jet propulsor models, namely PJP-0, PJP-1 and PJP-4, are used in current experimental and numerical investigation. The main particulars of the propulsors are listed in Table 1. The geometry of PJP-0 refers to Yu et al. (2019) and is scaled down by 0.8 times according to the experiment conditions of the cavitation tunnel. As shown in Figure 1, the pump-jet propulsor consists of the duct, the rotor, and the stator situated upstream of the rotor. The three propulsors differ from each other only in the geometry of the rotor near the tip, as shown in Figure 2. The design of rotor-tip geometry is expounded below.

Table 1. Main particulars of pump-jet propulsor models.

	Symbol	Unit	PJP-0	PJP-1	PJP-4
Number of rotor blades	Z_R	-	5	5	5
Number of stator blades	Z_S	-	7	7	7
Diameter of rotor	D_R	mm	235	235	235
Hub ratio	-	-	0.25	0.25	0.25
Pitch ratio at 0.7R	-	-	1.38	1.38	1.38
Width of tip clearance	-	mm	0.8	0.8	0.8
Tip rake	-	mm	0	7.1	-7.1

Figure 1. The pump-jet propulsor model.

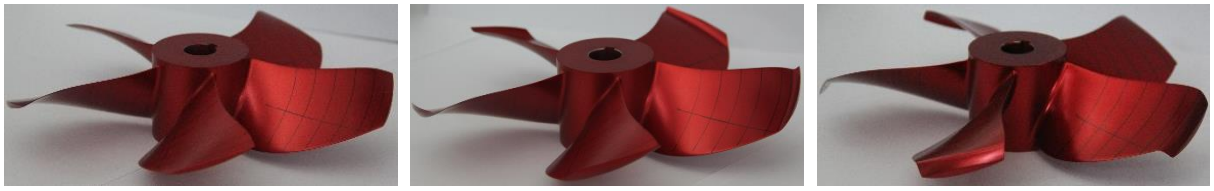

(a) PJP-0 (b) PJP-1 (c) PJP-4

Figure 2. The rotors of the pump-jet propulsor models.

PJP-1 and PJP-4 are obtained by increasing or decreasing the rake of the prototype propulsor, PJP-0, beyond 95% tip-radius. A nonlinear distribution of rake, Δx, as defined in Equation (1), is added to the rotor blade sections of PJP-0 for PJP-1 and subtracted from PJP-0 for PJP-4. The maximum of Δx is 3% of the rotor diameter. As shown in Figure 3, the rotor-tip of PJP-1 was made curved towards blade face side, while that of PJP-4 was bended towards the back side beyond 95% tip-radius.

$$\Delta x(r) = 0.03 D_R \left(20\frac{r}{R} - 19 \right)^2 \qquad (0.95 \le r/R \le 1) \tag{1}$$

where R is the tip radius and equals to $D_R / 2$.

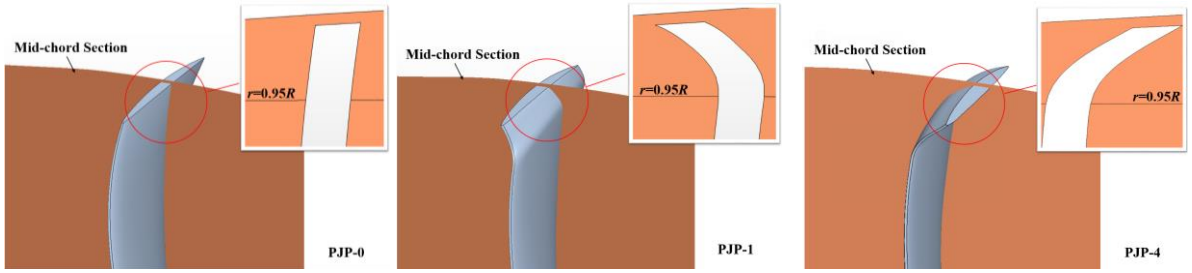

(a) PJP-0 (b) PJP-1 (c) PJP-4

Figure 3. The rotor-tip geometries.

3. Measurement of Fluctuating Pressures

3.1. Experimental setup

The measurement of fluctuating pressures on the inner surface of the duct was carried out in the cavitation tunnel of Shanghai Ship and Shipping Research Institute (SSSRI). The dimensions of the test section are 600 mm × 600 mm × 2600 mm. The maximum velocity at the inlet is 12 m/s, and the static pressure at propeller shaft centerline ranges from 10 kPa to 200 kPa.

Figure 4 (a) shows the installation of the pump-jet propulsor and pressure transducers in the cavitation tunnel. The rotor model is fixed to the J25 propeller dynamometer, which consists of a built-in shaft integrated with measuring units for propeller thrust and torque. The stator blades and duct are integrated and fixed to the stationary shaft casing of the propeller dynamometer. As shown in Figure 4 (b), the fluctuating pressures are measured by CYG505ALMF micro pressure transducers, which are of cylindrical shape and 5 mm in diameter. The measuring range is 0~500 kPa and accuracy class is 0.5%FS.

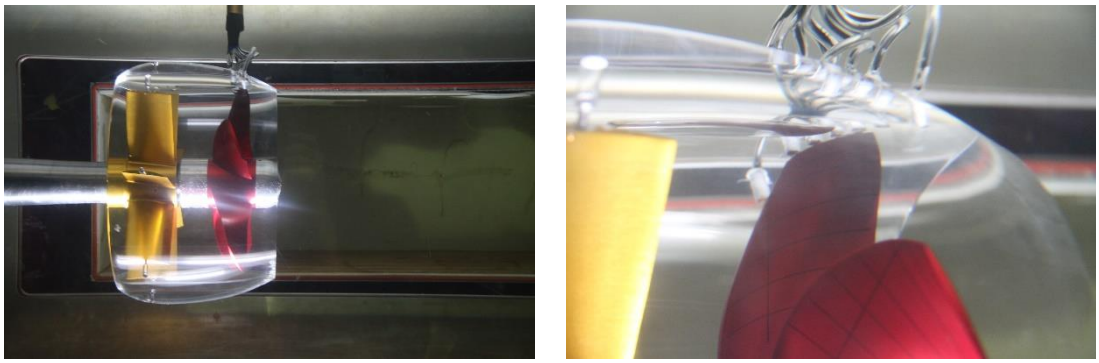

(a) (b)

Figure 4. Installation of the pump-jet propulsor and pressure transducers in the cavitation tunnel.

As illustrated in Figure 5, five micro pressure transducers, P1 through P5, are embedded in the duct wall, where the pressure sensing surfaces of them are flush with the inner surface of the duct. To investigate the effect of tip clearance flow on pressure fluctuation, the equally spaced transducers on the duct surface are aligned with the nose-tail line of the tip surface, where P1 and P5 point to the leading-edge and trailing-edge of the tip surface, respectively. With this arrangement, a 'simultaneous' distribution of fluctuating pressures can be obtained. Note that, since the tip surface of each propulsor is slightly different in location relative to the duct from that of the others, the locations of pressure transducers are unique for each propulsor.

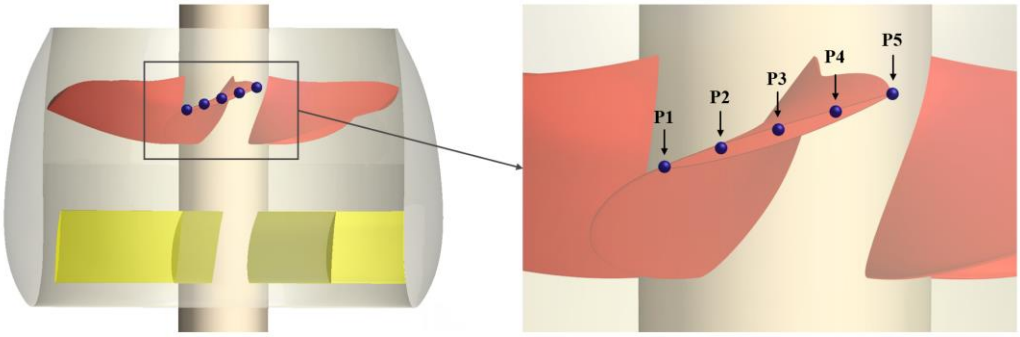

Figure 5. Arrangement of pressure transducers.

The fluctuating pressures are measured at specified operating conditions, where the rotational speed of the rotor is kept constant. The voltage signals from the transducers are sampled at a fixed frequency high enough to satisfy the requirement of Nyquist sampling theorem, for a duration long enough to perform FFT analysis. Then the sampled data are transformed to pressures via the calibration coefficients of the pressure transducers. The pressure, p, is expressed in terms of the pressure coefficient, C_p, which is defined as

$$C_p = \frac{p}{\frac{1}{2}\rho n^2 D_R^2} \tag{2}$$

where p_0 denotes the static pressure, and ρ denotes the density of water.

Except for the disturbances due to randomness of flow and the unsteady interactions among rotor and stator blade rows, which are both negligible for current configuration, the

fluctuating pressures are composed of harmonic components, with the blade passage frequency (BPF), nZ_R, as the base frequency. The fluctuating pressures are expressed as

$$C_p = a_0 + \sum_{j=1}^{\infty} a_j \cos\left(jZ_R \omega t + \varphi_j \right) \tag{3}$$

where a_0 denotes the time-average of C_p, $a_j \left(j = 1,2,...,\infty \right)$ denotes the amplitude of the j^{th} harmonic, or j times BPF component; and ω denotes the circular frequency, $\omega = 2\pi n$. Usually the amplitudes of fluctuating components attenuate as j increases. The 1st through 5th harmonics are adopted to evaluate the 'total' amplitude of fluctuating pressures, a, as follows (He and Wang, 1987),

$$a = \sqrt{\sum_{j=1}^{5} j a_j^2} \tag{4}$$

3.2. Analysis of measured data

The fluctuating pressures were measured at J=0.63 and J=0.77 in non-cavitating uniform inflow, where J is the advance ratio. The rate of revolution, n, was fixed at 18 s^{-1}. The Reynolds number at 0.7R ranges between 6×10^5 and 10^6. The voltage signals from the pressure transducers were sampled at 4096 Hz for 15 seconds in each condition and transformed to pressure data. For the three propulsors with different rotor-tip geometry, the time histories of fluctuating pressures at P1 through P5 within one revolution as well as the fluctuation amplitudes a_1 through a_5 of each time history are compared in Figures 6 and 7. The distributions of total fluctuating pressure amplitudes at P1 through P5 are shown in Figure 8.

As seen in Figures 6 and 7, the measured pressures fluctuate in five cycles each revolution, where each cycle corresponds to the passing period of a rotor blade. The pressure variations are similar among P1 through P3, but quite different both in form and magnitude at P4 and P5, indicating that the tip-leakage flow becomes complicated and the TSVs become weak as it goes towards the trailing edge. As shown in the right columns of Figures 6 and 7 and in Figure 8, at P1 through P3, *i.e.* from the leading edge to mid-chord, the fluctuating pressure amplitudes of PJP-1 are much higher than those of PJP-0, but those of PJP-4 are lower than those of PJP-0, indicating that raking the rotor tips forward, *i.e.* towards blade back side, is favorable for supressing the pressure fluctuations on duct surface. The mechanism will be explored via CFD simulations.

Despite of the difference in thrust loading between J=0.63 and J=0.77, the time histories of measured pressures are quite similar in the two conditions, except that the curves are smoother at J=0.77, where the tip-leakage flow is theoretically weaker since the thrust loading is lighter than that at J=0.63. However, as shown in Figure 9, for the same propulsor, the ratios of total amplitude of fluctuating pressure to the rotor thrust, a / K_{TR}, are mostly close to each other between J=0.63 and J=0.77. This result seems to indicate that a, the total fluctuation amplitude of C_p, is roughly proportional to the thrust coefficient of the rotor, K_{TR}, when the blades are moderately loaded. Possibly the relation can be utilized

to predict the total amplitudes of fluctuating pressures based on the data available in one operating condition to another.

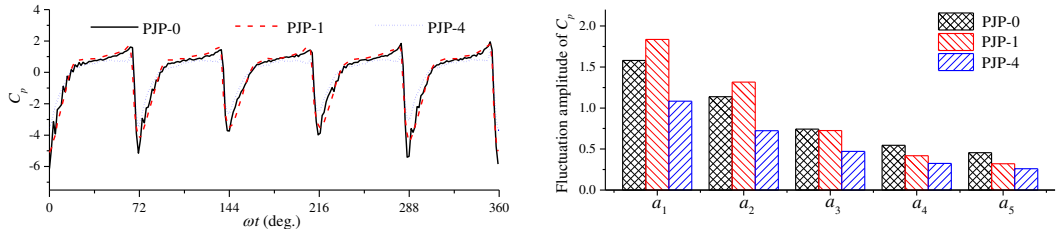

(a) P1

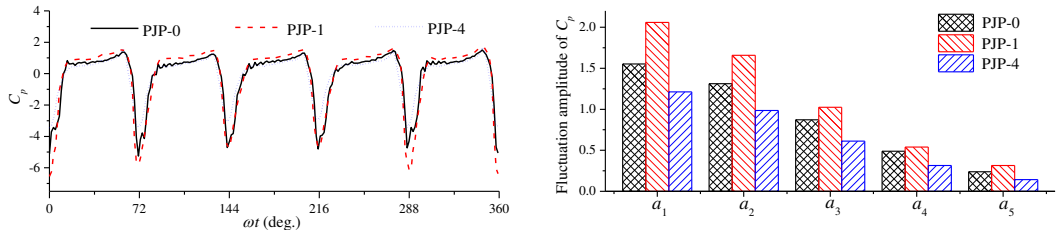

(b) P2

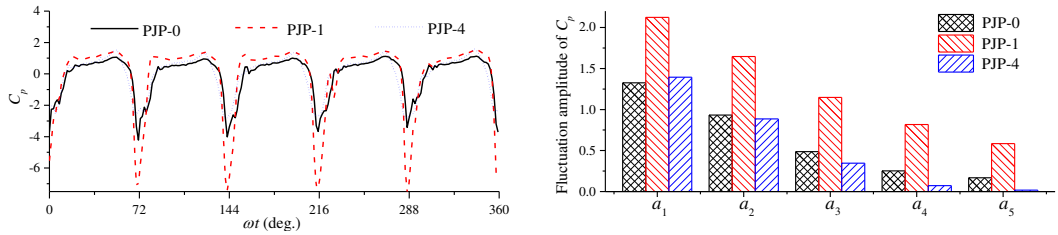

(c) P3

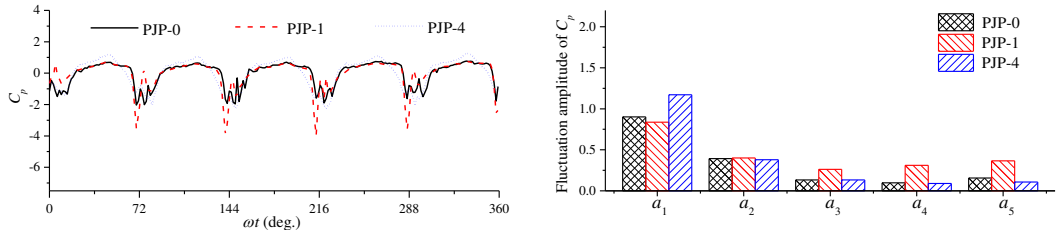

(d) P4

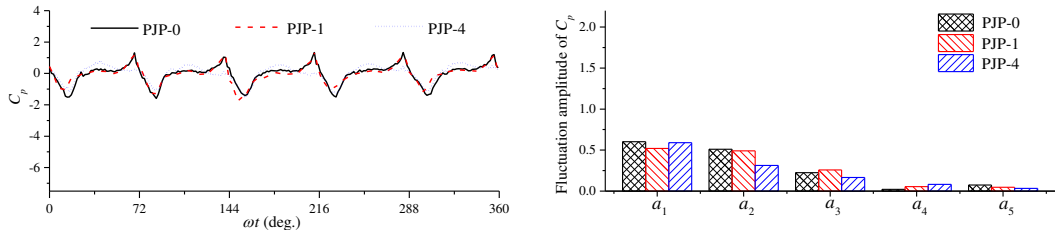

(e) P5

Figure 6. Comparison of measured time histories (left) and fluctuation amplitudes of C_p (right), J=0.63.

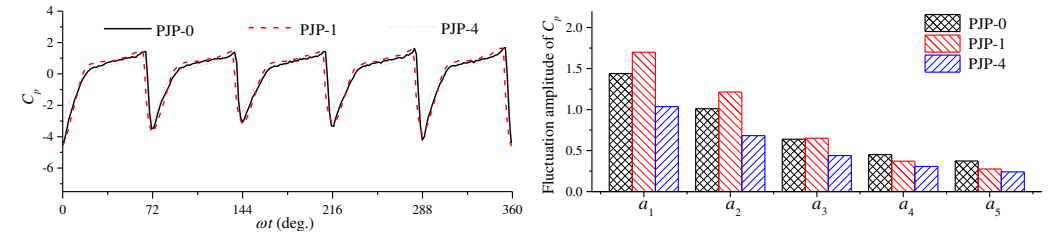

(a) P1

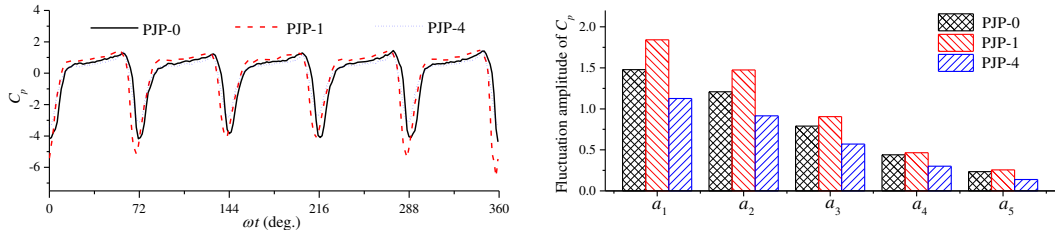

(b) P2

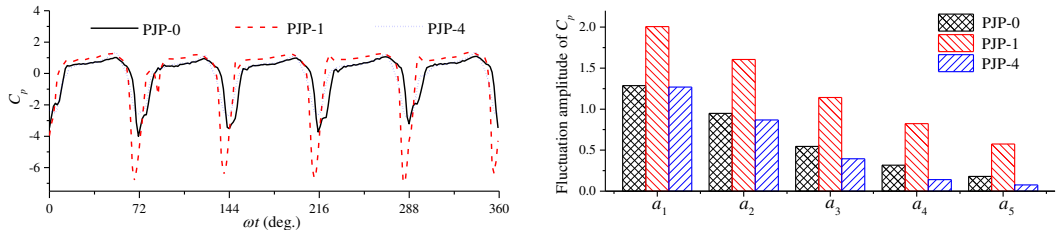

(c) P3

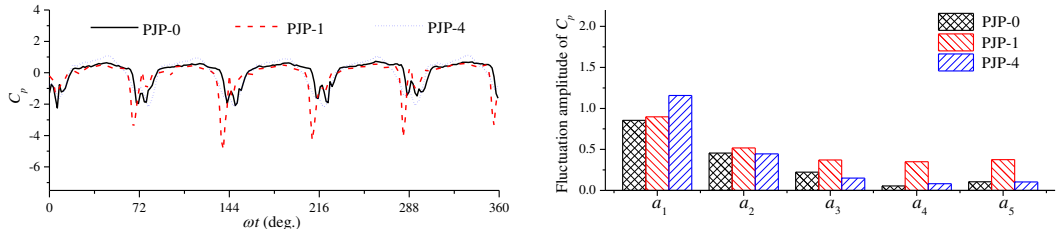

(d) P4

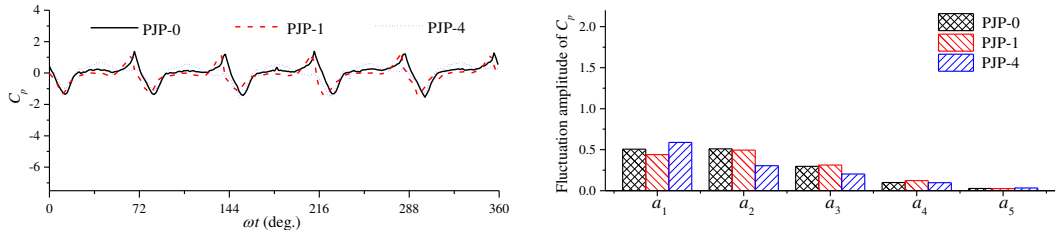

(e) P5

Figure 7. Comparison of measured time histories (left) and fluctuation amplitudes of C_p (right), J=0.77.

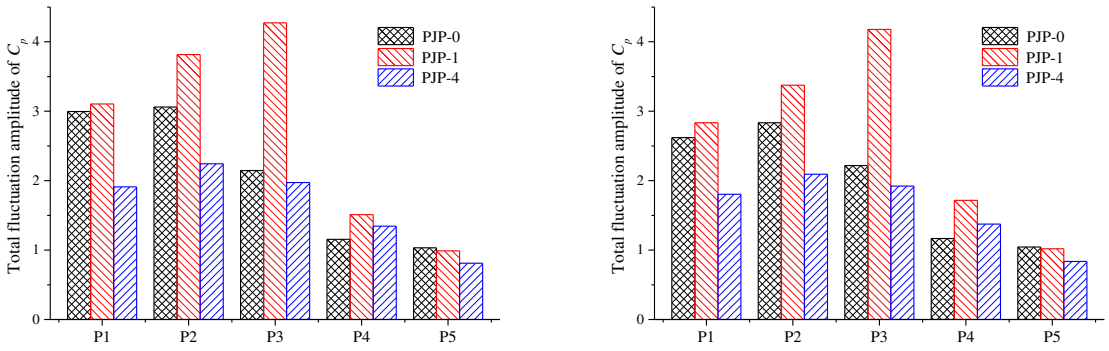

(a) J=0.63 (b) J=0.77

Figure 8. Comparison of total fluctuation amplitudes of C_p.

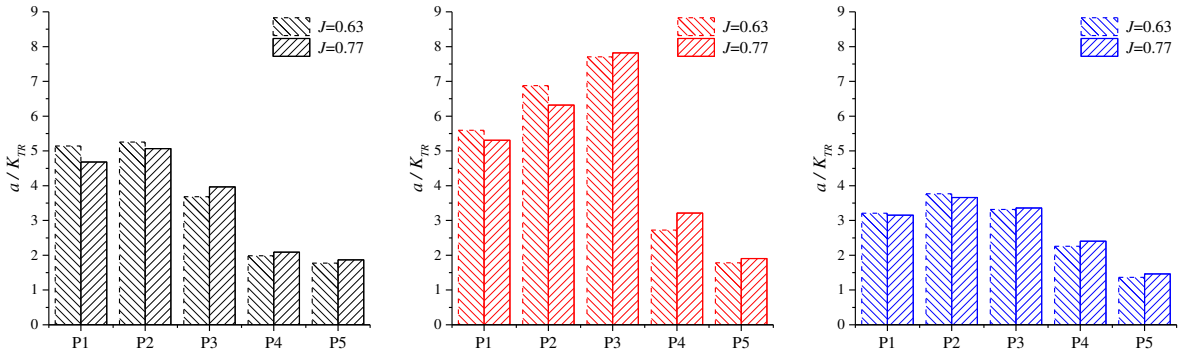

(a) PJP-0 (b) PJP-1 (c) PJP-4

Figure 9. Comparison of total amplitudes of pressure fluctuation relative to rotor thrust, a / K_{TR}.

4. Numerical Investigation of Excitation Forces

In addition to the experimental study, CFD simulations are conducted to enable a detailed investigation into the impacts of rotor-tip geometry on duct-surface fluctuating pressures and the resultant unsteady forces acting on different components of the pump-jet propulsor.

4.1. CFD modeling approach

The numerical simulations are based on the solution of the unsteady Reynolds-Averaged Navier-Stokes (RANS) equations using the SST k-ω model for turbulence closure. The RANS simulations were carried out using the CFD software STAR-CCM+.

As illustrated in Figure 10, the computational domain is a cylinder, of which the cross section is the same in geometry and size as those of the test section of the cavitation tunnel. However, the domain is much longer than its physical counterpart, in order that the flow is fully developed when reaching at the propulsor and at the outlet. The rotor disk is located at 2100 mm downstream of the velocity inlet, and 3360 mm upstream of the pressure outlet.

The computational domain is divided into the stationary sub-domain shown in blue and the rotating sub-domain shown in red, see Figure 10. The rotating sub-domain contains the rotor blades and is bounded by part of the duct's inner surface, as illustrated in Figure11. Both sub-domains are discretized into block-structured hexahedral cells with the grid generator ICEM CFD 17.2. Using the parameters of the grid model validated in Ji et al. (2021), similar grids are generated for the pump-jet propulsors with different rotor-tip geometries. The 0.8 mm tip-clearance is discretized with 25 layers of grids in order to better predict the tip-clearance flow, as shown in Figure 12. Very thin boundary-layer grids are used to ensure y^+~1 on body surfaces of the propulsor, so that the viscous sub-layer flow is resolved by using the all-y^+ wall treatment. Figure 13 is a typical distribution of the wall y^+. The total number of cells is about 27.2 million for the entire computational domain, where about 9.3 million cells are used to discretize the rotating sub-domain.

A uniform inflow is specified normal to the velocity inlet, and the flow speed is the same as that in the experiments, as the size and rotational speed of the propulsor models in CFD are the same as those in physical model tests. All the body surfaces are set as smooth, non-slip surfaces. The rate of revolution of the rotor is set at 18 s^{-1} and the time step size is 0.703°, which corresponds to 512 time steps each revolution.

Figure 10. The computational domain.

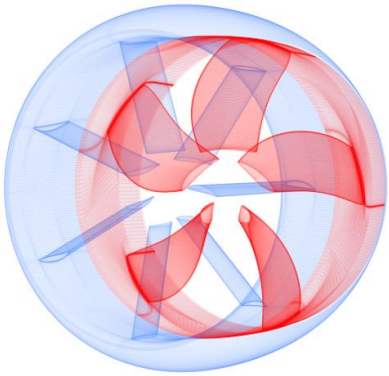

Figure 11. Grids on propulsor surfaces.

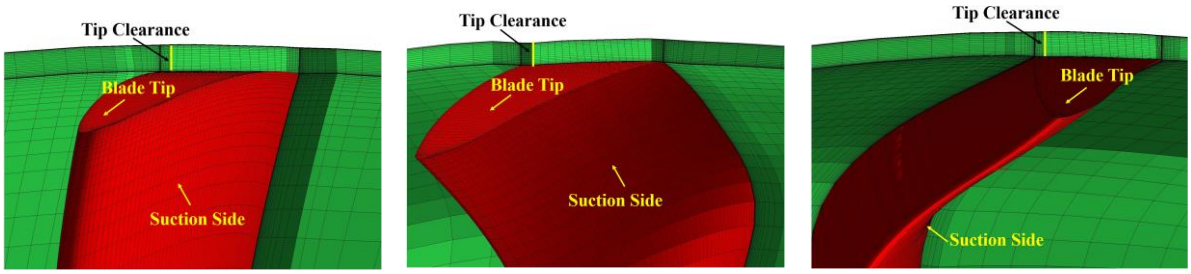

(a) PJP-0 (b) PJP-1 (c) PJP-4

Figure 12. Grids in the tip clearance.

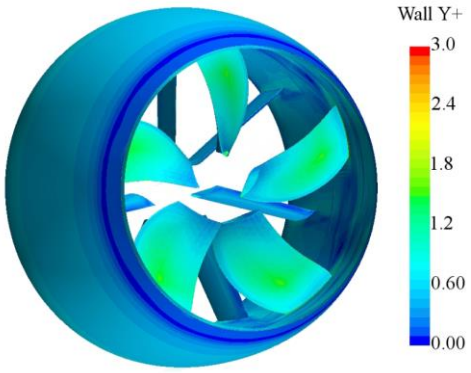

Figure 13. Typical distribution of wall y^+ on propulsor surfaces.

4.2. Analysis of numerical results

4.2.1. Fluctuating pressures and tip-clearance flow

Figure 14 compares the RANS simulation and experimental measurement results of time history and total fluctuation amplitude of duct-surface pressures at J=0.77. The comparison at J=0.63 is omitted for brevity as it is similar to the case of J=0.77. The simulated variations of pressure with time and at different locations agree reasonably well with those measured, though the total amplitudes are over-predicted at P2 due to the error more likely resulting from the most intense flow separation near this position.

Taking PJP-0 as an example, Figure15 and 16 displays the instantaneous duct-surface pressure distribution and tip-clearance flows by iso-surfaces of Ω-method (Liu et al., 2019) colored with pressure at three different instants. The three instants, A-A_1, B-B_1 and C-C_1, correspond to the moments marked by red lines in Figure 14(a) with equal interval during one passing period of a rotor blade. It can be seen from Figure 15 that the lowest pressure occurs at the instant when the nose-tail line is just passing over the pressure monitoring points P1 through P5. After the motion reaches the stability, the vortex structure and strength, and their influence on duct surface as well, change little at different time instants, as shown in Figure 15 and 16. Thus it is feasible to compare the flow patterns and pressure of the three propulsors at any same instant.

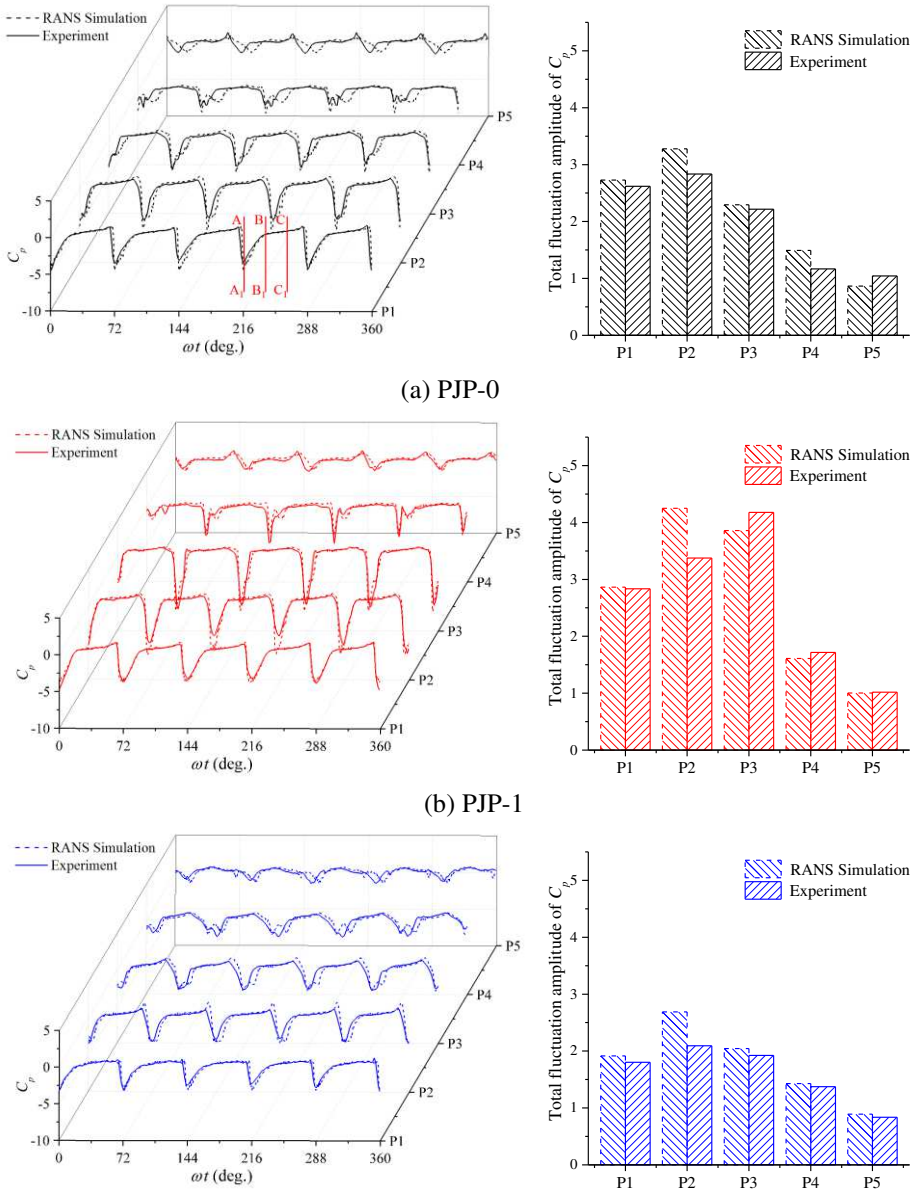

Figure 14. Comaprison of RANS simulation and experimental measurement results of time histories (left) and total fluctuation amplitudes (right) of duct-surface pressures, J=0.77.

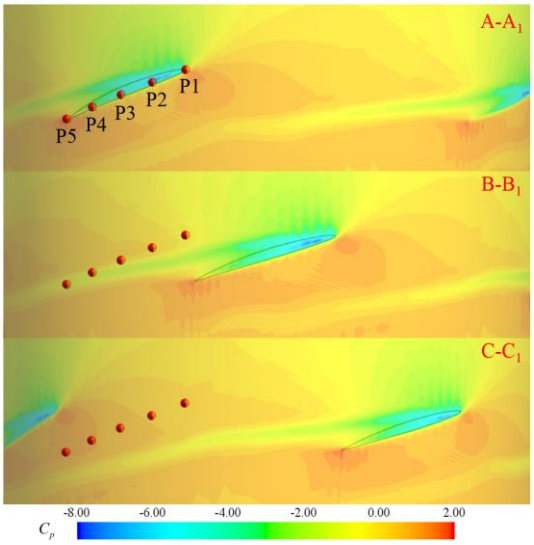

Figure 15. The duct-surface pressure distribution of PJP-0 at three time instants, J=0.77.

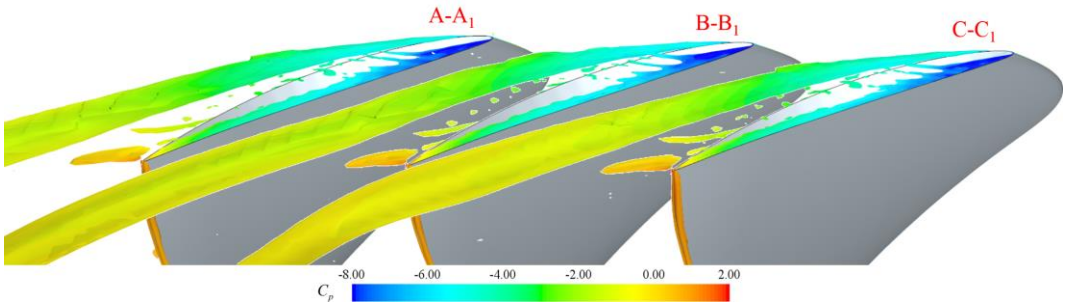

Figure 16. The tip-clearance flows by iso-surfaces of Ω-method of PJP-0 at three time instants, Ω=0.52, J=0.77.

Figure 17 shows the RANS simulation results of duct-surface pressure distributions (in the left column) and tip-clearance flows (in the right column) of the three propulsors with different rotor-tip geometries. The streamlines, both along the downstream development and in the sections perpendicular to the nose-tail line of tip surface, were captured at the instant when the nose-tail line was just passing over the five pressure monitoring points and colored with pressure. The sections are placed at 25%, 50% and 75% of the chord length where corresponds to the arrangements of P2, P3 and P4. On the inner surface of the duct, low pressures occur in the region swept by the part from the leading edge to the mid-chord of the rotor-tip surface. Correspondingly, the total amplitudes of pressure fluctuations shown in Figure 14 are higher at P1, P2 and P3. By comparing the pressure and flow results in Figure 17, it is clear that the low-pressure magnitudes on the duct surface are positively correlated with the strength of TSVs in the tip clearance. The TSVs, which emerge around the corner of blade face side and the tip surface due to flow detachment, became intensified in the case of PJP-1 because the above-mentioned corner became sharp when the tip was raked downstream and are weakened in the case of PJP-4 when the tip was raked upstream. The pressure fluctuations can be effectively reduced by weakening the TSVs. Based on present experimental and numerical results, raking the rotor-tips towards blade back side, *i.e.* the case of PJP-4, is favorable for suppressing the pressure fluctuations.

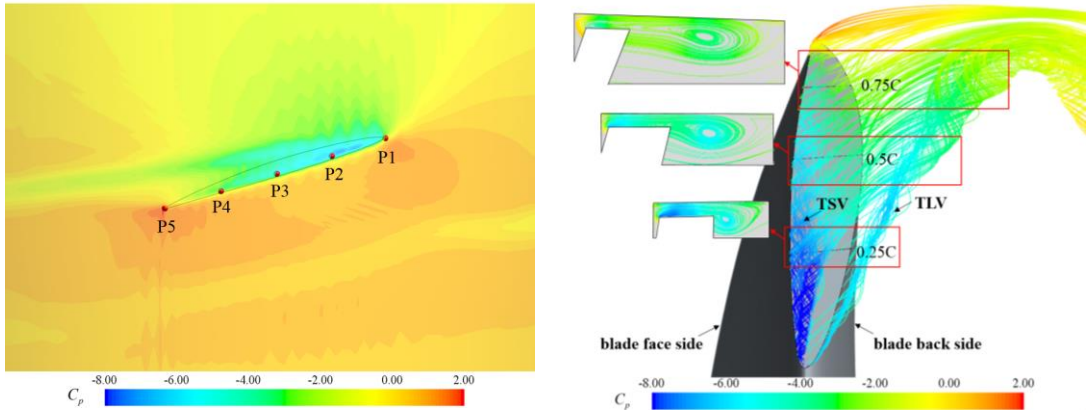

(a) PJP-0

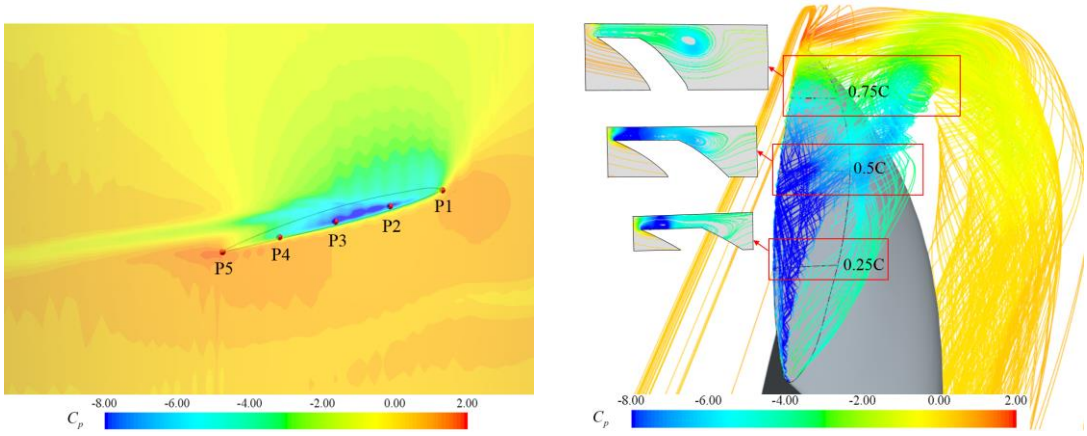

(b) PJP-1

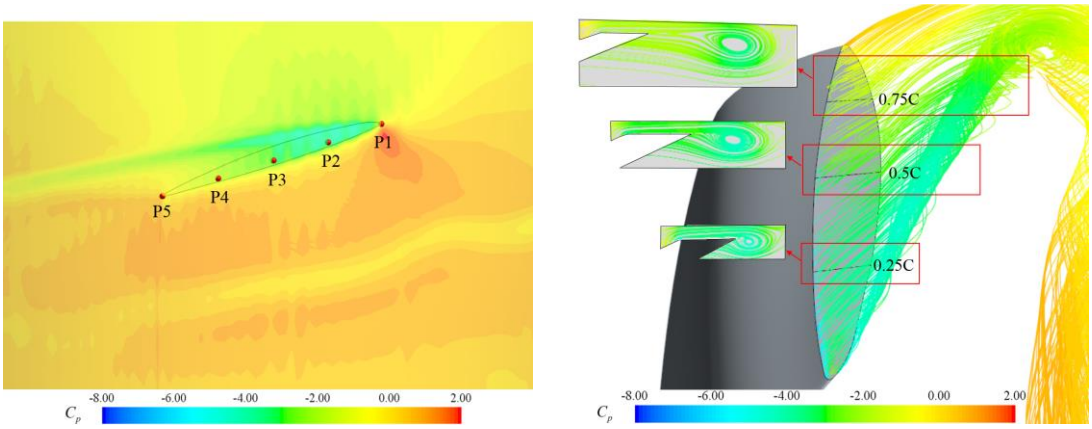

(c) PJP-4

Figure 17. Comparison of RANS simulation results of duct-surface pressure distribution (left) and tip-clearance flow (right) among the pump-jet propulsors with different rotor-tip geometries, J=0.77.

The vortex identification Ω-method is also emplyed to identify the vortices and Figure 18 compares the distributions of vortices on *xoz* plane between three rotors, at six intervals in the period of one rotor blade. There are mainly two typical vortices, stator wake vortices and tip-clearance vortices, the latter of which blends with the shedding vortices from the

duct trailing edge when developing out of the duct (Huang et al., 2021). The stator wake vortices are generally limitedly affected by rake and relatively strengthed slightly by the forward rake. The downstream TLVs which have escaped the tip clearance are clearly captured in the *xoz* plane in Figure 18, as explained by PJP-0 in Figure 19. In the area relatively upstream, PJP-1 and PJP-4 both suppress the beginning of TLVs but for different reasons. Due to backward rake, the primary TLV of PJP-1 detaches from the suction side much later downstream than PJP-0. While for PJP-4, the reason probably is the weakened flow separation near the leading edge by raking the rotor-tip towards the back side. However, as TLVs develop downstream, forward rake results in even stronger vortices.

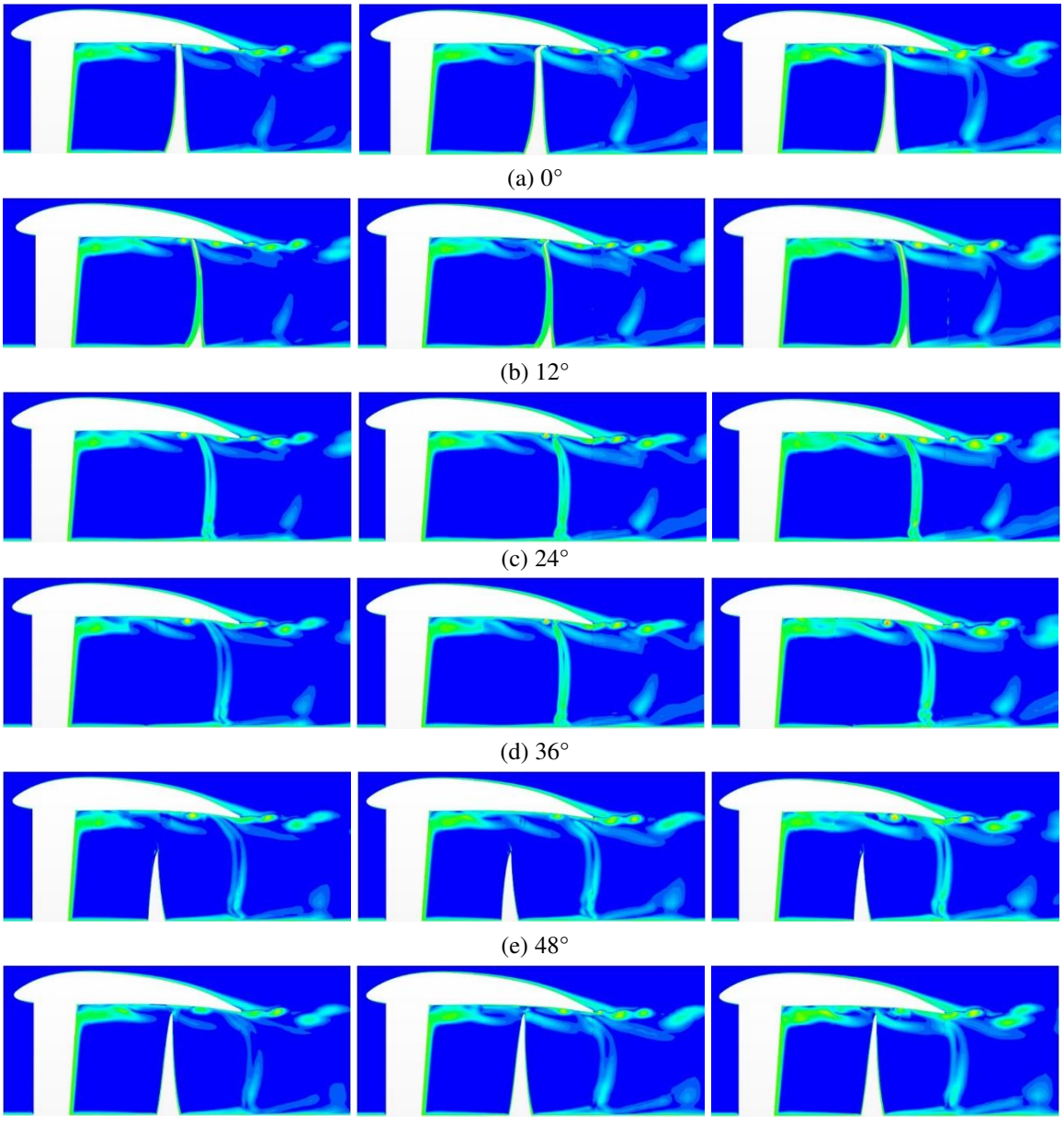

(a) 0°

(b) 12°

(c) 24°

(d) 36°

(e) 48°

(f) 60°

Figure 18. Comparison of the distributions of Ω (ranging from 0 to 1) on *xoz* plane between the three rotors (from left to right: PJP-0, PJP-1, PJP-4), J=0.77.

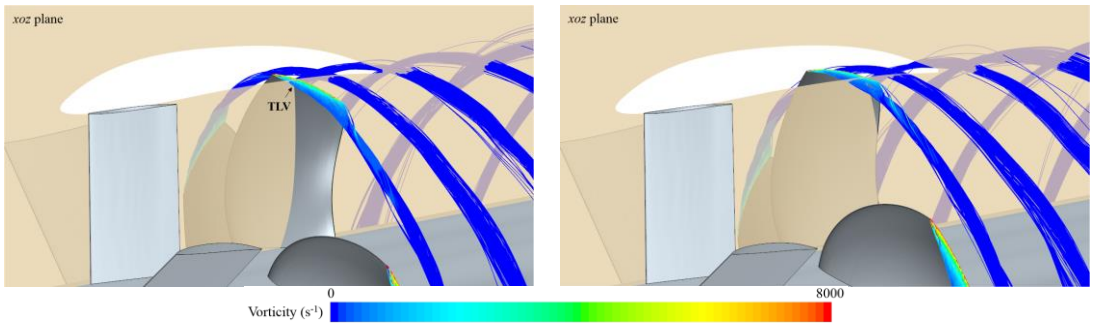

(a) 0° (a) 12°

Figure 19. Geometry and TLVs captured by *xoz* plane at different intervals, PJP-0, *J*=0.77.

4.2.2. Resultant unsteady forces

The fluctuating pressures acting on duct, stator, and rotor surfaces result in the resultant unsteady forces which can excite structural vibrations of the pump-jet propulsor components under suitable conditions. The fluctuating forces are mainly due to the non-uniform wake and rotor/stator interaction. Only the latter is investigated in current research.

The resultant unsteady forces due to rotor/stator interaction act on all components of the pump-jet propulsor at the discrete frequencies equaling to knZ_R $(k=1,2,...,\infty)$, where nZ_R is the blade passage frequency (BPF) of the rotor. However, not all the harmonics exist unless certain conditions are fulfilled. According to Strasberg et al. (1976) and Rao et al. (2013), axial force components occur only when $kZ_R = qZ_S$, while horizontal and vertical force components occur only when $kZ_R = qZ_S \pm 1$, where k and q are positive integers, Z_R and Z_S are the number of rotor and stator blades, respectively. The unwanted harmonic components can be avoided with an appropriate combination of Z_R and Z_S; however, it often happens that low-frequency components would occur in horizontal and vertical forces when a low-frequency component of the axial force is avoided, and vice versa. Usually, low-frequency components are relatively high in amplitude and damp slowly, compared with high-frequency ones.

For the pump-jet propulsors under investigation, the rotors and stators are five-bladed (Z_R=5) and seven-bladed ($Z_S=7$), respectively. The lowest frequency of axial force component equals to 7 times nZ_R. However, it was found that the amplitude of this component was too small to be resolved with present CFD simulation approach. Thus only the thrust and torque of one single rotor blade ($\tilde{F}_x^R$ and $\tilde{M}_x^R$), which fluctuate at qnZ_S $(q=1,2,...,\infty)$, are compared between the three rotors in Figure 20 and 21. On the other hand, theoretically the first and second lowest frequencies in horizontal and vertical force components should be 3 and 4 times nZ_R, respectively. Figure 22 shows the CFD simulation results of time history and frequency spectrum of $F_y^{D\&S} / F_x^R$ for PJP-0 at *J*=0.77, where $F_y^{D\&S}$ is the resultant horizontal force acting on the duct and the stator (as they are structurally integrated as an assembly), and F_x^R is the time-averaged thrust of the rotor. The results are the same for vertical force component due to the periodicity of flow in circumferential direction. The horizontal force fluctuates in five cycles each revolution, influenced by rotor blades and the numerical results agree perfectly with theoretical ones in terms of frequency, as seen in Figure 22.

As shown in Figure 20 and 21, the fluctuation amplitude of $\tilde{F}_x^R$ and $\tilde{M}_x^R$, the resultant axial force and moment acting on one single rotor blade, are compared at first five stator blade passing frequencies, nZ_S. The total amplitudes of PJP-1 drops 20% ~ 40% compared to PJP-0 and those of PJP-4 are up by 25% ~ 40% over PJP-0. It can be known that the backward rake is beneficial to weakening the axial unsteady forces and moments, which is probably because of larger distance between stator and rotor, while forward rake exerts the opposite influence. However, the axial unsteady forces of the whole rotor due to rotor/stator interaction are much weaker than those of one single blade and vertical fluctuating forces.

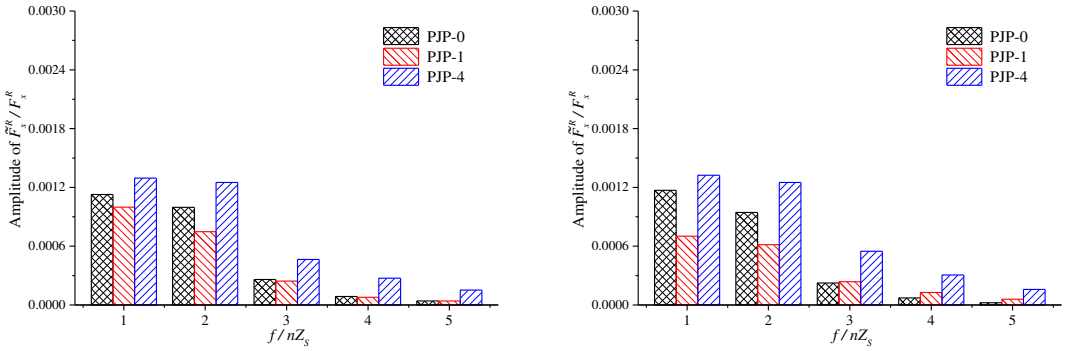

(a) J=0.63 (b) J=0.77

Figure 20. Influences of rotor-tip rake on the fluctuation amplitude of resultant axial force acting on one single rotor blade.

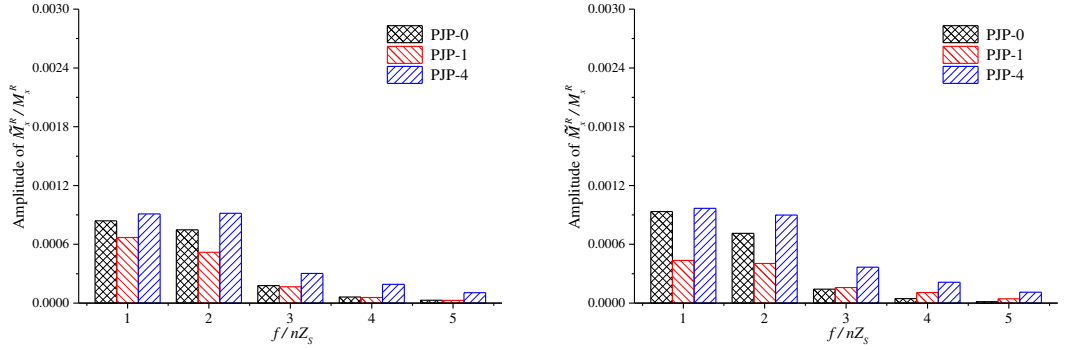

(a) J=0.63 (b) J=0.77

Figure 21. Influences of rotor-tip rake on the fluctuation amplitude of resultant axial moment acting on one single rotor blade.

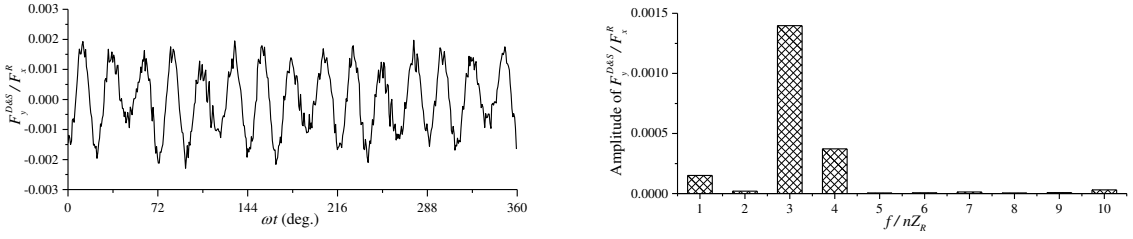

Figure 22. Time history (left) and frequency spectrum (right) of the resultant horizontal force acting on the duct and the stator for PJP-0, J=0.77.

In Figure 23, the influences of raking the rotor tips on the fluctuation amplitude of $F_y^{D\&S}$, the resultant horizontal force acting on the duct and the stator, are shown. In both operating conditions (J=0.63 and J=0.77) investigated, compared to PJP-0, the fluctuation amplitudes of $F_y^{D\&S}$ increase for PJP-1 and decrease for PJP-4. The total amplitudes at 3 and 4 times nZ_R of PJP-1 are 20% ~ 70% higher than those for PJP-0 and the difference is more significant at smaller advance ratio, that is, the larger attack angle. The above amplitudes of PJP-4 are about 30% ~ 50% lower than those for PJP-0. This trend between the three propulsors agrees with the pressure fluctuation results on the duct. However, both PJP-1 and PJP-4 tend to increase the amplitude of F_y^R, the resultant horizontal force acting on the rotor, as shown in Figure 24. Compared with PJP-0, the fluctuating F_y^R of PJP-1 worsens more significantly while the amplitudes of PJP-4 increase slightly at 4 times nZ_R. Moreover, the fluctuation of $F_y^{D\&S}$ is relatively more sensitive to the attack angle. It can be inferred that horizontal and vertical fluctuating forces acting on the duct and stator are more heavily influenced by tip clearance flows which are more intense with the larger attack angle. After all, these results indicate that raking the rotor tips towards blade back sides is favorable for reducing the resultant horizontal and vertical fluctuating forces acting on the duct and stator of the pump-jet propulsor, though slightly harmful to those acting on the rotor.

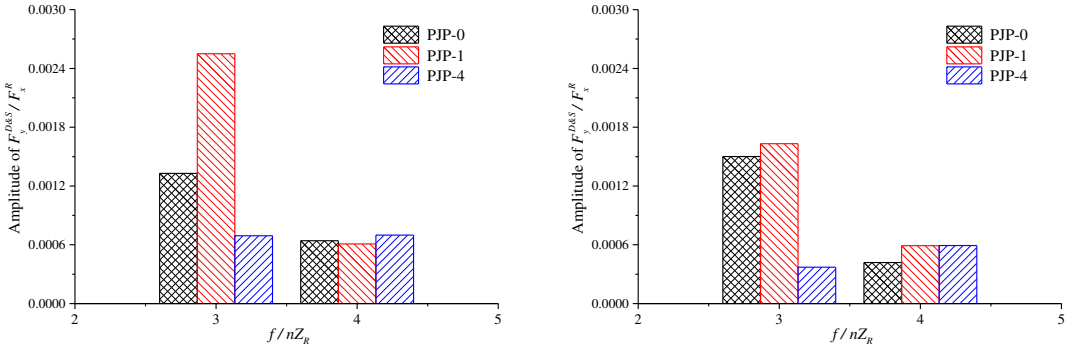

(a) J=0.63 (b) J=0.77

Figure 23. Influences of rotor-tip rake on the fluctuation amplitude of resultant horizontal force acting on the duct and the stator.

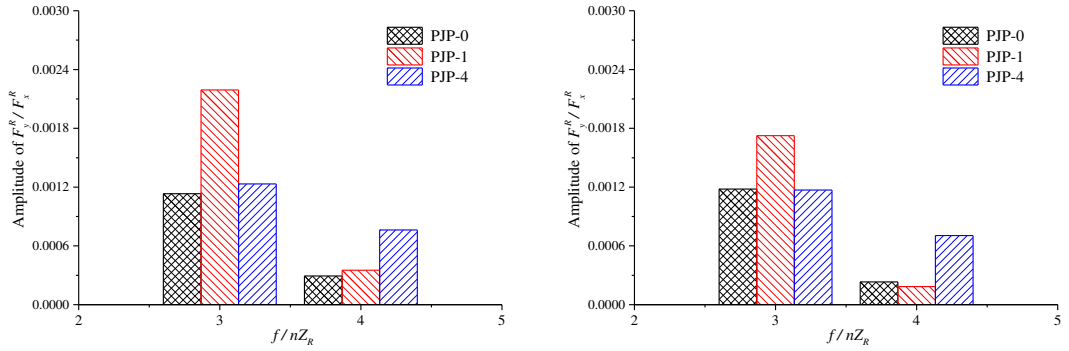

(a) J=0.63 (b) J=0.77

Figure 24. Influences of rotor-tip rake on the fluctuation amplitude of resultant horizontal force acting on the rotor.

5. Conclusions

In this paper, the effects of raking the rotor tips on duct-surface fluctuating pressures and the resultant unsteady forces acting upon the pump-jet propulsor are investigated via physical model experiments and viscous-flow CFD simulations. The conclusions are drawn as follows,

(1) The time histories of dimensionless pressures are quite similar at different advance ratios and the total fluctuation amplitude of pressure is roughly proportional to the thrust coefficient of the rotor.

(2) The high amplitudes of fluctuating pressures are attributable to the strong tip separation vortices (TSVs) detaching from the corner of blade face side and the tip surface. Both experimental and numerical results indicate that the fluctuating pressures can be reduced by raking the rotor tips towards blade back side (PJP-4).

(3) Further analysis of the CFD results indicates that, due to the interaction between the 5-bladed rotor and 7-bladed stator, the fluctuation amplitudes of resultant horizontal (and vertical) forces acting on the duct/stator assembly is significantly reduced as rake decreases and increased as rake increases. Backward rake results in much higher fluctuation amplitude of horizontal (and vertical) unsteady forces of the rotor than forward rake. Though fluctuation amplitudes of resultant axial forces acting on one single rotor blade are increased as rake decreases, those on the whole rotor are much weaker compared to vertical fluctuating forces.

The last two findings suggest that raking the rotor tips towards the back side is an effective solution to reducing the excitation forces due to the rotor/stator interaction, while raking towards the face side may strengthen TSVs and exert a negative effect on resultant pressure fluctuations and unsteady forces.

Compliance with Ethical Standards

Conflict of interest: The authors declare that they have no conflict of interest.

Ethical approval: This article does not contain any studies with human participants or animals performed by any of the authors.

Informed consent: Informed consent was obtained from all individual participants included in the study.

Funding: The current research was funded by the National Key Project of China for Strengthening Fundamental Research, Grant No. 2019-JCJQ-ZD-016-00.

REFERENCES

Arndt, R.E.A., Arakeri, V.H., Higuchi, H., 1991. Some observations of tip-vortex cavitation. Journal of Fluid Mechanics. 229, 269-289.

Chen, E., Ma, Z., Zhao, G., Li, G., Yang, A., Nan, G., 2016. Numerical investigation on vibration and noise induced by unsteady flow in an axial-flow pump. Journal of Mechanical Science & Technology. 30(12), 5397-5404.

Cheng, H., Long, X., Ji, B., Peng, X., Farhat, M., 2020. Suppressing tip-leakage vortex cavitation by overhanging grooves. Experiments in Fluids. 61, 159.

Decaix, J., Dreyer, M., Balarac, G., Farhat, M., Münch, C., 2018. RANS computations of a confined cavitating tip-leakage vortex. European Journal of Mechanics-B/Fluids. 67, 198-210.

González, J., Parrondo, J., Santolaria, C., Blanco, E., 2006. Steady and unsteady radial forces for a centrifugal pump with impeller to tongue gap variation. ASME. Journal of Fluids Engineering. 128(3), 454-462.

Guo, Q., Zhou, L., Wang, Z., 2016. Numerical evaluation of the clearance geometries effect on the flow field and performance of a hydrofoil. Renewable Energy. 99, 390-397.

He, Y.S., Wang, G.Q., 1987. Propeller excitation forces. Shanghai Jiao Tong University Press, in Chinese.

Huang, Q.G., Li, H., Pan, G., Dong X.G., 2021. Effects of duct parameter on pump-jet propulsor unsteady hydrodynamic performance. Ocean Engineering. 221, 108509.

Ji, X.Q., Dong, X.Q., Li, W., Yang, C.J., Francis, N., 2019. Numerical investigation of tip geometry on the tip-clearance flow features of a pump-jet propulsor. Proceedings of the VIII International Conference on Computational Methods in Marine Engineering, Gothenburg, Sweden. 576-587.

Ji, X.Q., Dong, X.Q., Yang, C.J., 2021. Attenuation of the tip-clearance flow in a pump-jet propulsor by thickening and raking the tips of rotor blades: A numerical study. Applied Ocean Research. 113, 102723.

Karn, A., Arndt, R.E.A., Hong, J., 2016. An experimental investigation into supercavity closure mechanisms. Journal of Fluid Mechanics. 789, 259-284.

Li, N., Zhang, L.G., Wang, Z.L., Cai, Y.L., 2014. Numerical analysis of influence of tip vane width on pulse pressure of pump's shroud. Noise and Vibration Control. 34(5), 34-37, in Chinese.

Liu, C., Gao, Y.S., Dong, X.R., Wang, Y.Q., Liu, J.M., Zhang, Y.N., Cai, X.S., Gui, N., 2019. Third generation of vortex identification methods: Omega and Liutex/Rortex based systems. Journal of Hydrodynamics. 31(2), 205-223.

Liu, Y., Tan, L., Wang, B., 2018. A review of tip clearance in propeller, pump and turbine. Energies. 11(9), 2202.

Liu, Y., Tan, L., 2018. Method of C groove on vortex suppression and energy performance

improvement for a NACA0009 hydrofoil with tip clearance in tidal energy. Energy. 155, 448-461.

Liu, Y., Tan, L., 2020. Method of T shape tip on energy improvement of a hydrofoil with tip clearance in tidal energy. Renewable Energy. 149, 42-54.

Sonawat, A., Kim, S., Ma, S.B., Kim, S.J., Lee, J.B., Yu, M.S., Kim, J.H., 2022. Investigation of unsteady pressure fluctuations and methods for its suppression for a double suction centrifugal pump. Energy. 252, 124020.

Strasberg, M., Breslin, J.P., 1976. Frequencies of the alternating forces due to interactions of contra-rotating propellers. Journal of Hydronautics. 10, 62-74.

Rao, Z.Q., Li, W., Yang, C.J., 2014. Theoretical analysis and numerical simulation of unsteady interaction forces on ducted propeller with pre-swirl stators. Journal of Ship Mechanics. 18, 45-53, in Chinese.

Tan, L., Xie. Z.F., Liu, Y., Hao, Y., Xu, Y., 2018. Influence of T-shape tip clearance on performance of a mixed-flow pump. Proceedings of the Institution of Mechanical Engineers, Part A, Journal of Power and Energy. 232(4), 386-396.

Ye, J.M., Sun, D.P., Shi, B.Y., 2021. Research on controlling tip flow of pump-jet propeller based on rectangular groove structure. Shipbuilding of China. 62(3), 70-84, in Chinese.

Yu, H., Duan, N., Hua, H., Zhang, Z., 2020. Propulsion performance and unsteady forces of a pump-jet propulsor with different pre-swirl stator parameters. Applied Ocean Research. 100, 102184.

Yu, H., Zhang, Z., Hua, H., 2019. Numerical investigation of tip clearance effects on propulsion performance and pressure fluctuation of a pump-jet propulsor. Ocean Engineering. 192, 106500.

Zhang, N., Liu, X., Gao, B., Wang, X., Xia, B., 2019. Effects of modifying the blade trailing edge profile on unsteady pressure pulsations and flow structures in a centrifugal pump. International Journal of Heat and Fluid Flow. 75, 227-238.